

Fear Processing and Social Networking in the Absence of a Functional Amygdala

Supplemental Information

Volunteers

Demographical and Neuropsychological Characteristics

With less than 300 reported cases since its initial description, lipoproteinosis of Urbach-Wiethe (LP; syn. Urbach-Wiethe disease or Hyalinosis cutis et mucosae; OMIM 247100), LP is a rare autosomal recessive genodermatosis typified by cutaneous, mucosal and visceral deposits of periodic acid-Schiff (PAS)-positive hyaline (glycoprotein) material that pathognomonically presents itself in early infancy through hoarse cries due to infiltration of the vocal cords (1). Intracranial mineralizations occur in up to 50 – 75% of LP patients and may be slowly progressive in nature, such that the clinical phenotype is often complicated by epilepsy (2). Whereas patient 1 has never suffered epileptic seizures, patient 2 suffered a first grand-mal seizure at age 12, which led to diagnosis of LP and subsequent diagnosis of her twin sister. Due to pregnancy, patient 2 has stopped her anticonvulsive therapy with a 900-mg daily dose of valproate in 2006. Both patients report pre-epileptic auras that occur up to twice a month. Grown up in a shared family environment in a rural residential area in southern Germany, the twins have completed 13 years of education and been in fulltime employment since. They are 36 years of age, married, have children, display an average IQ (HAWIE-R: patient 1, 101; patient 2, 96), and perform relatively unimpaired across a wide range of neuropsychological and psychopathological measures (3), which is consistent with their previously reported disease profiles (4-6) (for a characterization of South-African LP patients see also (7, 8)). Controls had a mean age of 33.7 years (SEM = 0.9 years), reported an average of 14.1 years of education (SEM = 0.7 year), had no current or history of neurological or psychiatric illness, and performed within the normal range on measures of visual attention (including processing speed, rule compliance, quality of performance, and task switching) (Table S1).

Table S1. Demographics and neuropsychological data in the control group

	Age	Education	BDI	TMT-A*	TMT-B*	D2*
MS	33.7	14.1	2.6	103.1	100.4	104.8
SEM	0.9	0.7	0.6	1.5	2.5	2.2

MS, mean score; SEM, standard error of the mean; BDI, Beck Depression Inventory; TMT-A, Trail-making Test: subtest A; TMT-B, Trail-making Test: subtest B; D2, test of attention.

*Presented are standard scores (mean = 100, standard deviation = 10).

Molecular Genetics

LP is caused by mutations in the extracellular matrix protein 1 gene (*ECM1*) located on chromosome 1q21. The biological functions of *ECM1* are not yet fully elucidated, but it encodes an extracellular protein involved in dermal differentiation, endochondral bone formation and angiogenesis (9,10). Exons 6 and 7 are the most common sites for *ECM1* mutations in LP (Table S2). Mutations inside exon 7 are usually associated with a milder mucocutaneous clinical phenotype, since exon 7 is only present in the alternative splicing variant ECM1a (long form of the protein composed of 540 amino acids), but not in ECM1b (short form of the protein composed of 415 amino acids) (9,10). To determine the underlying mutation in the twins, whole-genomic DNA was extracted from 10 ml aliquots of EDTA-anticoagulated venous blood using a salting-out method. A set of 7 primer pairs was used to amplify 7 polymerase chain reaction (PCR) fragments covering the 10 exons of the *ECM1* gene from the twins' DNA samples. Direct sequencing of the purified PCR products was carried out on an automatic sequence analyzer by a commercial sequencing service (MWG Biotech, Ebersberg, Germany). Sequence reads were confirmed manually, and the sequences were assembled using the SeqMan module of the Lasergene 8.0 software (DNASTAR, Madison, WI). The twins showed the same genotype in all sequenced regions. In exon 7 a novel homozygous missense mutation was found, resulting in an exchange of a highly conserved tryptophan to arginine: (c.709T>C; p.W237R; Figure S1). The alignment of proteins belonging to the *ECM1* family confirmed that tryptophan 237 is highly conserved, pointing to the potential pathogenic relevance of the p.W237R mutation (Figure S2, red mark on top).

Table S2. Reported mutations of the extracellular matrix protein 1 gene (*ECM1*)

Missense point mutations			
Accession number*	Amino acid change	Change in cDNA	Reference
CM076161	V10G	29T>G	Chan <i>et al.</i> (2007) (9)
CM031960	R53X	157C>T	Hamada <i>et al.</i> (2003) (10)
CM076163	Q74X	220C>T	Chan <i>et al.</i> (2007) (9)
CM076156	Q95X	283C>T	Chan <i>et al.</i> (2007) (9)
CM076157	Q114X	340C>T	Chan <i>et al.</i> (2007) (9)
CM031961	W160X	480G>A	Hamada <i>et al.</i> (2003) (10)
CM031962	F167I	499T>A	Hamada <i>et al.</i> (2003) (10)
CM076159	F167L	499T>C	Chan <i>et al.</i> (2007) (9)
CM053847	Q197X	589C>T	Lupo <i>et al.</i> (2005) (11)
CM076158	L210P	629T>C	Chan <i>et al.</i> (2007) (9)
CM062588	C220G	658T>G	Wang <i>et al.</i> (2006) (12)
CM031963	R243X	727C>T	Hamada <i>et al.</i> (2003) (10)
CM045741	E248X	742G>T	Chan <i>et al.</i> (2004) (13)
CM111331	C269Y	n.a.	Salih <i>et al.</i> (2011) (14)
CM020676	Q276X	826C>T	Hamada <i>et al.</i> (2002) (1)
CM020677	Q346X	1036C>T	Hamada <i>et al.</i> (2002) (1)

CM020678	W359X	1077G>A	Hamada <i>et al.</i> (2002) (1)
CM076162	Y369C	1106A>G	Chan <i>et al.</i> (2007) (9)
CM076164	R416X	1246C>T	Chan <i>et al.</i> (2007) (9)
CM062587	R476X	1426C>T	Wang <i>et al.</i> (2006) (12)
CM076160	R481X	1441C>T	Chan <i>et al.</i> (2007) (9)
Mutations leading to splicing errors			
	Intervening sequence	Donor/Acceptor Location	
CQ076616	1	ds +1	Chan <i>et al.</i> (2007) (9)
CQ056751	1	ds +1	Horev <i>et al.</i> (2009) (15)
CQ076617	7	ds +1	Chan <i>et al.</i> (2007) (9)
CQ076618	8	ds +1	Chan <i>et al.</i> (2007) (9)
Small deletions			
		Position in cDNA	
CD097880		240_241del2	Horev <i>et al.</i> (2009) (15)
CD032106		244del1	Hamada <i>et al.</i> (2003) (10)
CD032107		507del1	Hamada <i>et al.</i> (2003) (10)
CD032108		735_736del2	Hamada <i>et al.</i> (2003) (10)
CD032109		785del1	Hamada <i>et al.</i> (2003) (10)
CD032110		893del1	Hamada <i>et al.</i> (2003) (10)
CD020850		1019del1	Hamada <i>et al.</i> (2003) (10)
CD076785		1257del1	Chan <i>et al.</i> (2007) (9)
CD076783		1300_1301del2	Chan <i>et al.</i> (2007) (9)
CD097879		1395del1	Horev <i>et al.</i> (2009) (15)
CD076784		1433del1	Chan <i>et al.</i> (2007) (9)
Small insertions			
CI020895		506dup1	Hamada <i>et al.</i> (2002) (1)
CI032144		542_543ins2	Hamada <i>et al.</i> (2003) (10)
CI032145		1192dup1	Hamada <i>et al.</i> (2003) (10)
Small indels			
	Insertion		
CP035427	tt	93_94del2ins2	Chan <i>et al.</i> (2003) (16)
CX045846	agaaccaaactgaa	541_542del2ins15	Teive <i>et al.</i> (2004) (17)
CX067587	ggctgattccggct	541_542del2ins15	DiGiandomenico <i>et al.</i> (2006) (18)
Gross deletions			
		Description	
CG024877		1163bp incl. ex. 9-10	Hamada <i>et al.</i> (2002) (1)
Gross insertions			
	Insertion		
CN094935	62bp c.1209_1210		Nasir <i>et al.</i> (2009) (19)
HN080001	62bp c.1209_1210		Hameed <i>et al.</i> (2009) (20)

*adapted from Stenson *et al.* (2003) (21)

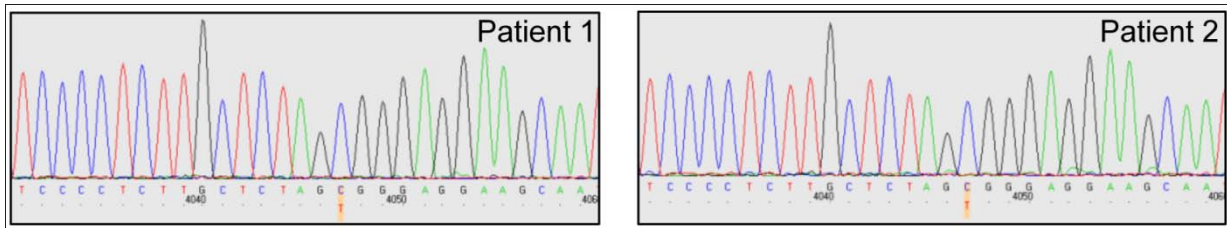


Figure S1. Fragment of the genomic sequence from exon 7 of the extracellular matrix protein 1 gene (*ECM1*) from patient 1 (left panel) and patient 2 (right panel). The homozygous c.709T>C missense mutation leading to an exchange of a highly conserved tryptophan at position 237 to arginine is indicated with the yellow box.

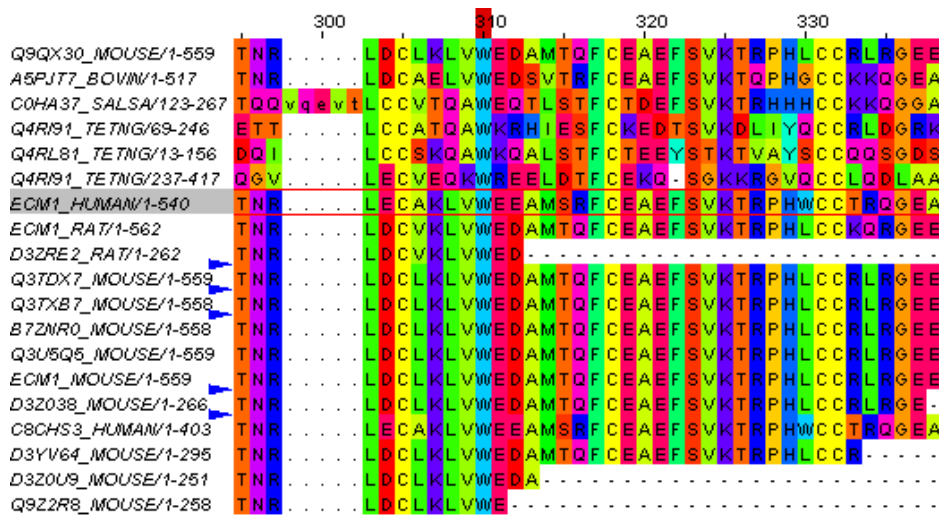


Figure S2. Alignment of proteins of the extracellular matrix protein 1 gene (*ECM1*) family (PF05782). The position of tryptophan 237 (here position 310, red mark on the top) is highly conserved among proteins belonging to the *ECM1* family. This is an indication for a probable functional relevance of Trp237 and pathogenicity of the novel p.Trp237Arg *ECM1* missense mutation detected in the twins. The following proteins were aligned: Q9QX30_MOUSE [Mus musculus (Mouse)] Extracellular matrix protein (559 residues); A5PJT7_BOVIN [Bos taurus (Bovine)] *ECM1* protein (517 residues); C0HA37_SALSA [Salmo salar (Atlantic salmon)] Extracellular matrix protein 1 (535 residues); Q4RI91_TETNG [Tetraodon nigroviridis (Green puffer)] Chromosome 8 SCAF15044, whole genome shotgun sequence (498 residues); Q4RL81_TETNG [Tetraodon nigroviridis (Green puffer)] Chromosome 21 SCAF15022, whole genome shotgun sequence (163 residues); *ECM1_HUMAN* [Homo sapiens (Human)] Extracellular matrix protein 1 (540 residues); *ECM1_RAT* [Rattus norvegicus (Rat)] Extracellular matrix protein 1 (562 residues); D3ZRE2_RAT [Rattus norvegicus (Rat)] Putative uncharacterized protein *ECM1* (437 residues); Q3TDX7_MOUSE [Mus musculus (Mouse)] Putative uncharacterized protein (559 residues); Q3TXB7_MOUSE [Mus musculus (Mouse)] Putative uncharacterized protein (558 residues); B7ZNR0_MOUSE [Mus musculus (Mouse)] *Ecm1* protein (558 residues); Q3U5Q5_MOUSE [Mus musculus (Mouse)] Putative uncharacterized protein (559 residues); *ECM1_MOUSE* [Mus musculus (Mouse)] Extracellular matrix protein 1 (559 residues); D3Z038_MOUSE [Mus musculus (Mouse)] Putative uncharacterized protein *Ecm1* (266 residues); C8CHS3_HUMAN [Homo sapiens (Human)] Truncated extracellular matrix protein 1 (403 residues); D3YV64_MOUSE [Mus musculus (Mouse)] Putative uncharacterized protein *Ecm1* (295 residues); D3Z0U9_MOUSE [Mus musculus (Mouse)] Putative uncharacterized protein *Ecm1* (251 residues); Q9Z2R8_MOUSE [Mus musculus (Mouse)] Extracellular matrix protein (434 residues).

Structural Imaging

T1-weighted structural magnetic resonance imaging (MRI) scans of both twins were acquired on a 1.5 Tesla Siemens Sonata system (Siemens, Erlangen, Germany) using an MP-RAGE sequence (22). Sequence parameters were adjusted for an optimal white matter-gray matter-cerebrospinal fluid contrast (TR = 2200 ms, TE = 4.38 ms, TI = 1240 ms, flip angle = 20°). In addition to a standard 3D anatomical scan with 1.0 mm isotropic resolution (matrix size = 256 x 256, field-of-view (FoV) = 256, axial slices = 160) five volumes with a higher isotropic resolution of 0.8 mm (matrix size 256 x 256, FoV = 205, axial slices = 192) were acquired to improve the anatomical characterization of the amygdala lesions. To compensate for a decrease in the signal-to-noise ratio (SNR) due to the smaller voxel size (23) (1.0 mm isotropic resolution, SNR = 20; 0.8 mm isotropic resolution, SNR = 10) while keeping the high resolution, five averages in form of five separate co-registered one-average runs were acquired (24). The manufacturer-provided sequence was modified to output phase in addition to magnitude data. The five data-sets were complex averaged in order to achieve high noise suppression; from the averaged complex data magnitude and phase images were generated. Since X-ray computed tomography (CT) easily detects calcium and is the clinically preferred method of localizing intracranial calcifications, the twins were scanned on a 16-row-multidetector CT device (Brilliance 16, Philips, Best, The Netherlands) (collimation = 16 x 0.75 mm, slice thickness = 2 mm, slice increment = 1 mm, FoV = 220 mm, matrix size = 512 x 512, rotation time = 0.75 s, pitch = 0.688, 120 kV, tube current at 120 kV = 350 mAs). CT-MRI co-registration was carried out in PMOD 3.1 (PMOD Inc., Zurich, Switzerland) and manually adjusted. To obtain accurate anatomical information on the lesion extent in both twins, volumes of interest (VOIs) were defined and measured in the axial, coronal and sagittal planes at a fixed threshold of 160 Hounsfield units using the PMOD 3.1 isocontour tool. For visualization purposes, these CT-derived contours were superimposed onto MRI (Figure S3) and rendered in 3D (25). The extracted VOI volumes did not significantly differ between patients (patient 1, mean = 1.12 ccm; patient 2, mean = 1.15 ccm). Anatomical inspection of all scans (K.Z.) revealed complete destruction of the basolateral amygdala (BLA) and minor, but equivalent sparing of anterior amygdaloid and ventral cortical amygdaloid parts at a rostral level as well as lateral and medial parts of the central amygdaloid nucleus and the amygdalo-hippocampal area at more caudal levels in both twins (Figure S3).

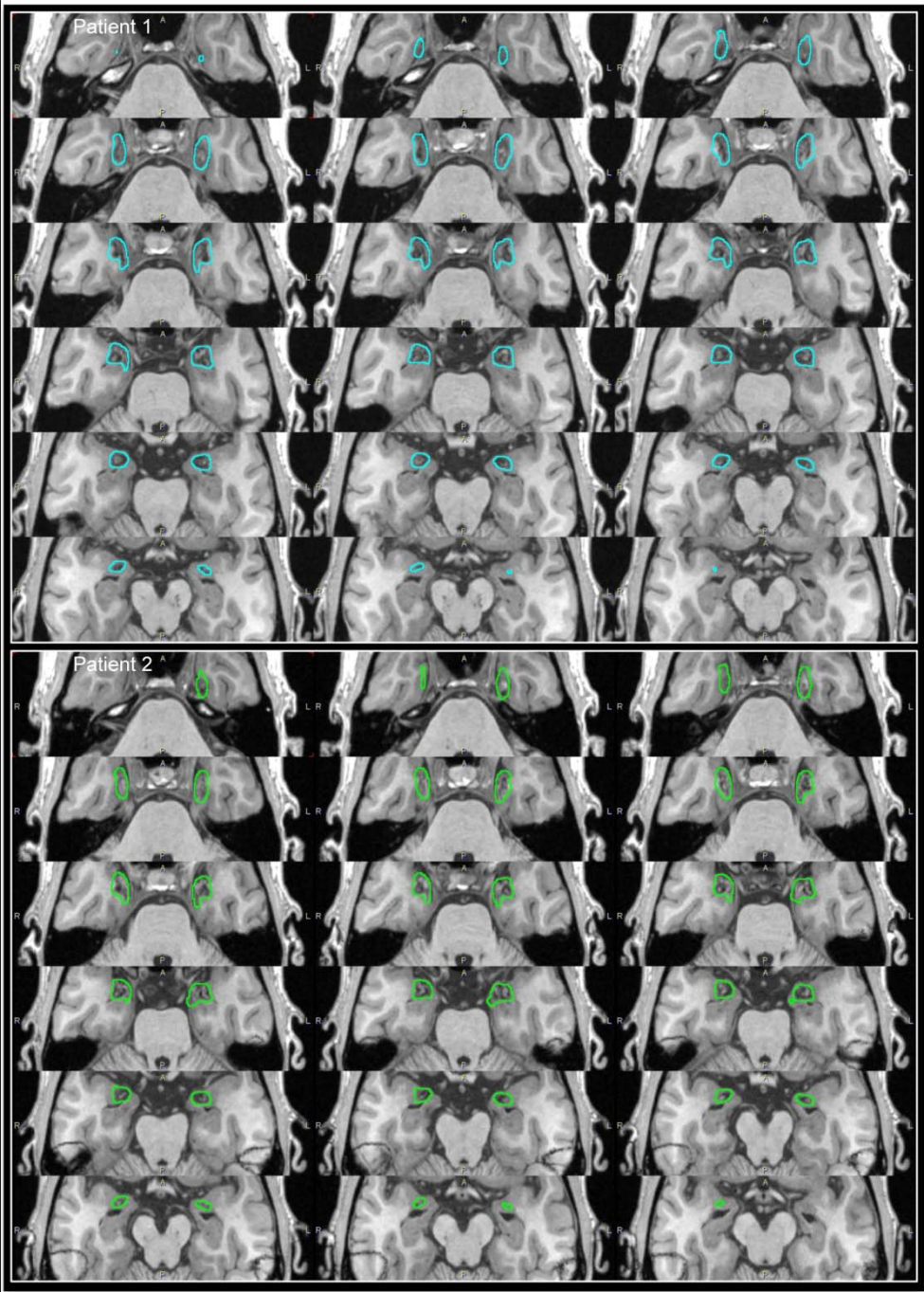


Figure S3. Axial (horizontal) magnetic resonance imaging sections of the anterior medial temporal lobes with color contours delineating the twins' calcification damage as detected by X-ray computed tomography scans. Blue contours index patient 1's calcification lesion, whereas green contours index patient 2's calcification lesion. L, left; R, right.

Experiment 1

All 15 controls and the twins were familiarized with the emotional labeling task by an example picture of each emotional category before the experiment. Additionally, 12 pictures of two individuals each showing the five emotional and a neutral expression were presented, and participants had to verbally label the emotions to practice the task. During this training period participants received feedback from the instructor whether their classification was correct, or not. Subsequently, 72 photographs were presented for 1.5 s, and after each picture the question ‘Which emotion has been shown?’ occurred on-screen for 3 s. Subjects were required to answer verbally, and their responses were voice-recorded. A fixation cross was shown for 10–15 s (average 12.5 s) between trials. Patients and controls did not differ in the amount of missed trials, and therefore missed trials (on average less than one trial per person) were excluded from further analysis. Throughout the experiment electrodermal activity (EDA) was measured by two EDA electrodes attached to the thenar and hypothenar of the non-dominant hand. The electrodes were filled with a non-hydrating NaCl paste, and a constant current of 0.5V was applied. A commercial system (Contact Precision Instruments, Cambridge, MA) was used for stimulus delivery and psychophysiological recordings. EDA was recorded at a sampling rate of 1000 Hz. Before the start of the experiment, 3 min of baseline EDA were recorded. To ensure a correct attachment and conductance of the electrodes, five acoustic startle probes (see also experiment 3) were randomly administered during this baseline measurement. Unfortunately, no reliable skin conductance response (SCR) to these startle probes could be measured in patient 2 due to transient skin ulcerations as a consequence of LP. In general, it is possible to record SCRs from patient 2. EDA was analyzed for each subject individually for a 10-s period from picture onset. An SCR was defined as the first wave in a time window between 1 and 4 s after stimulus onset with a phasic increase in conductance of more than 0.02 μ S. To normalize the data a log transformation was applied. Since the SCR amplitude did not significantly differ between the emotion categories (angry, disgusted, fearful, happy, neutral, and sad) in controls (all p values ≥ 0.06), the results have to be interpreted cautiously. The pattern of autonomic responses to the emotional faces was comparable between patient 1 and the control group, with the exception of disgusted faces (Figure S4). Patient 1 exhibited a smaller response to disgusted faces than controls. Notably, patient 1 as well as the control group generated the strongest SCR to fearful faces. This result further supports the hypothesis that patient 1 can at least partially compensate for her amygdala damage. However, the autonomic responses have to be interpreted with caution, since the SCR amplitude did not significantly differ between the emotion categories in controls (all p values ≥ 0.06).

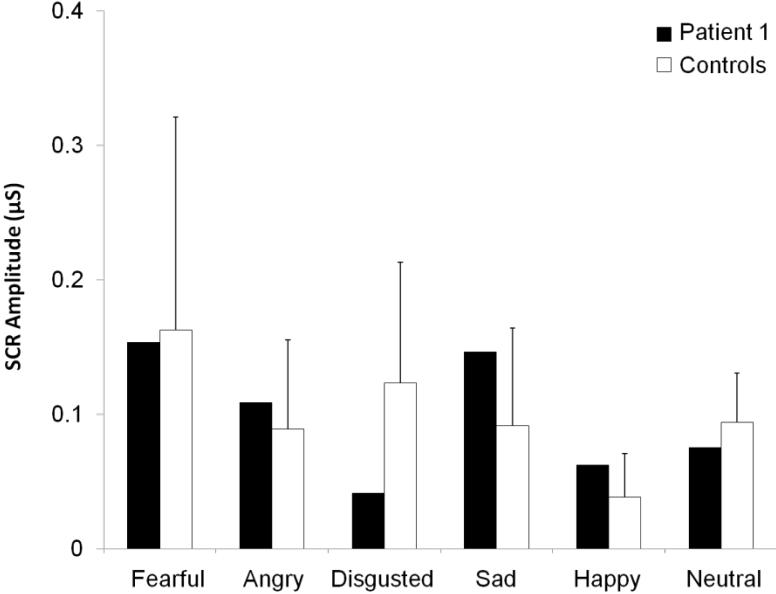


Figure 4. Skin conductance response (SCR) amplitudes (µS) for controls and patient 1. Error bars in the comparison group indicate the standard error of the mean (SEM).

Experiment 2

Functional MRI (fMRI) Paradigm

To stimulate the amygdala in controls and to trigger compensatory mechanisms in patient 1, we adopted a modified version of an established face perception task (26). Stimuli consisted of photographs depicting 40 individuals showing fearful facial expressions. In addition, photographs from the same individuals showing neutral and happy facial expressions were presented. Neutral faces were included to control for general differences in the neural correlates of face perception between patients and controls. Happy facial expressions were included to determine whether the compensatory mechanism selectively compensates for the recognition of fearful faces. The faces were selected from 'The Karolinska Directed Emotional Faces' database (27, 28). All stimuli were gray-scaled and equated for size and luminance. Stimuli were presented block-wise by means of liquid crystal display (LCD) video goggles (Nordic NeuroLab, Bergen, Norway) and Presentation 14 (Neurobehavioral Systems Inc., Albany, CA). Each stimulus was presented for 2625 ms, with an inter-stimulus interval (ISI) varying between 250 ms and 1500 ms, hence resulting in a mean block length of 14.5 s. Each block comprised four stimuli from the same emotional category (fearful, happy, or neutral). In total, 10 blocks of each fearful, happy, and neutral faces were presented. The sequence of blocks was randomized; blocks were separated by a low-level baseline during which a fixation cross in the center of the screen was presented. Subjects had to press a button in response to each face to assure stimulus processing and completed two runs of the task; for each run, 296 dynamic scans were recorded; the first five volumes were discarded to allow for T1 equilibration effects. Each run had a mean duration of approximately 15 min. To exclude control subjects with apparent brain pathologies, high-resolution anatomical MR images were acquired (T1-weighted 3D MPRAGE). Total MRI scanning time was approximately 40 min.

fMRI Data Acquisition

fMRI employing blood oxygenation level-dependent (BOLD) contrast was performed on a 1.5 Tesla Siemens Avanto MRI system (Siemens, Erlangen, Germany) using a T2*-weighted echoplanar EPI sequence (imaging parameters: TR = 3000 ms, TE = 50 ms, matrix size: 64 x 64, pixel size: 3.3 x 3.3 mm², slice thickness = 3.0 mm, distance factor = 10%, FoV = 210, flip angle = 90°, 35 axial slices). In addition, high-resolution anatomical images were acquired on the same scanner using a T1-weighted 3D MPRAGE sequence (imaging parameters: TR = 1660 ms, TE = 3.09, matrix size = 256 x 256, pixel size 1 x 1 mm², slice thickness = 1.0 mm, FoV = 256, flip angle = 15°, sagittal slices = 160).

fMRI Data Analysis

fMRI data were preprocessed and analyzed using SPM8 (Wellcome Trust Centre for Neuroimaging, London, United Kingdom; <http://www.fil.ion.ucl.ac.uk/spm>) implemented in MATLAB

7 (The MathWorks Inc., Natick, MA). Images were corrected for head movement between scans by an affine registration (29). For realignment, a two-pass procedure was used, by which images were initially realigned to the first image of the time-series and subsequently re-realigned to the mean of all images. Mean images were normalized with the SPM8 MNI template (30, 31). All images were subsequently transformed into standard stereotaxic space and resampled at 3 x 3 x 3 mm voxel size. The normalized images were spatially smoothed using an 8-mm full-width half-maximum Gaussian kernel. Raw time series were detrended by the application of a high-pass filter (cut-off period, 128 s). Conditions (fearful, happy, neutral faces) were modeled by a boxcar function convolved with a hemodynamic response function (32). A single design matrix comprising contrasts of alternating intervals of the different blocks and movement parameters for both runs was created. Specific effects were assessed by applying appropriate linear contrasts to the parameter estimates of the experimental trials resulting in t-statistics for each voxel. To test whether the face-perception task led to amygdalar activity in the normal controls and thus had the capability of triggering compensatory responses in the twins, separate one-sample t-test for the conditions 'fearful faces' and 'happy faces' were computed. Because of the small size of the control sample and our *a priori* anatomical hypothesis, analyses were restricted to the bilateral amygdala, and regions of interest (ROIs) were anatomically defined using the WFU Pickatlas (Version 3.0), which provides a method for generating ROI masks based on the Talairach Daemon database (a detailed description of the WFU PickAtlas and the anatomical masks employed is given in (33-35)). The implemented atlases are located in Montreal Neurological Institute (MNI) space with dimensions of 91 × 109 × 91 sampled at 2-mm intervals, corresponding to the SPM MNI templates. ROI-based one-sample t-tests were computed with a threshold of $p < 0.05$ and corrected for multiple comparisons (family-wise error, FWE), implemented in a small volume correction, based on the size of the bilateral amygdala ROI. To test if the compensatory mechanism involves supra-normal activity, separate two-sample t-tests (patient 1 vs controls, patient 2 vs controls) with pooled estimates of the error variance (36) for the conditions 'fearful faces', 'neutral faces' and 'happy faces' were computed. Because of no *a priori* hypotheses on the brain regions which might be involved in compensatory processes, whole-brain analyses were performed ($p < 0.05$ FWE-corrected for multiple comparisons). This analysis revealed higher activity in patient 1 compared to controls in the left premotor cortex face area (PFA) ($t = 11.12$, $p < 0.05$; cluster size = 4 voxel; maximum t-value in Talairach space at $x = -32$, $y = 9$, $z = 58$) for the fearful faces. No differences were found for the happy and neutral faces or for patient 2. For further analysis individual parameter estimates for the condition 'fearful faces' were extracted from a spherical ROI (radius = 10 mm) centered at the maximum t-value of the left PFA cluster. In comparison to controls, patient 1 displayed increased activity ($z = 5.24$, $p < 0.001$), whereas patient 2 ($z = 1.82$, $p = 0.068$) did not differ from controls. To analyze altered activity of the patients within the

fearful face-processing network with a higher sensitivity, parameter estimates for the following anatomically defined regions were extracted from the conditions 'neutral faces' and 'fearful faces': bilateral inferior frontal gyrus, bilateral fusiform gyrus, bilateral inferior parietal gyrus, bilateral medial frontal gyrus, and bilateral insula. These regions have been selected according to a recent meta-analysis on emotional face processing (37). Differences between patients and controls were analyzed using z-tests. Group statistics were performed on data sets obtained from 12 of 15 participants. One participant reported that she had felt uncomfortable during MRI acquisition, and two data sets showed severe head movement during scanning. Data sets from these participants were excluded from further analysis.

Experiment 3

The experiment contained 20 neutral and 20 negative (mostly fear-eliciting) stimuli with social content selected from the 'International Affective Picture System' (IAPS) (39). The following IAPS pictures were used as neutral stimuli: 2025, 2030, 2102, 2190, 2210, 2381, 2382, 2392, 2396, 2397, 2411, 2440, 2491, 2499, 2506, 2516, 2593, 4001, 4275, and 8311. The negative category contained: 2100, 2811, 3000, 3015, 3060, 3170, 6213, 6220, 6250.1, 6311, 6520, 6530, 6540, 6831, 8231, 9042, 9321, 9413, 9427, and 9452. Participants were administered the self-assessment manikin (SAM) (38) to obtain pleasure and arousal ratings for each stimulus on a scale ranging from 1 (minimum) to 9 (maximum) after the experiment (Table S3). In line with previous research of LP patients (39), the twins displayed reduced arousal ratings. The impairments were more severe in patient 2 who also assigned abnormally high valence ratings to negative pictures. A commercial system (Contact Precision Instruments, Cambridge, MA) was used to control the stimulus presentation and the psychophysiological recording. Subjects were seated approximately 100 cm in front of a computer screen in a slightly reclined chair with a headrest. Each participant viewed the pictures in a different, pseudo-random order. The pictures were presented for 5 s on-screen, with 7-17 s (average 12 s) intervals between them. A fixation cross was presented in the center of the screen during the ISI. A 70-dB white noise background was present throughout the experiment. The acoustic startle probe was a 50-ms burst of white noise (100 dB) with nearly instantaneous rise. It was delivered binaurally via headphones during 75% of the slices (15 neutral and 15 negative slices) at 300, 3000, and 4000 ms after picture onset. To reduce predictability, 15 ISIs were also accompanied by startle probes. Furthermore, the experiment started with the presentation of five startle probes in 2-s intervals to account for early habituation. Facial electromyographic (EMG) activity was recorded from two Ag/AgCl electrodes placed over the orbicularis oculi muscle below the left eye (placement as recommended by (40)). A ground electrode was placed behind the subjects' left ear. The EMG signal was digitized at a rate of 1000 Hz and amplified with a high-pass filter of 30 Hz and a low-pass filter of 500 Hz. The EMG data were rectified and smoothed by a 4-point moving average. Startle eyeblink reflex was calculated as the difference between the maximum increase of EMG activity in a time interval between 20 and 100 ms after startle probe onset and the mean EMG of the 50-ms baseline directly preceding the onset. All EMG data were z-transformed within subjects and then converted into T-scores to reduce between-subjects variability and skew. The EMG recordings were visually inspected, and a total of 6.7% of all trials were discarded because of excessive noise in the baseline interval or because the startle stimulus overlapped with spontaneous eye blinks. Three participants had to be excluded due to recording problems and/or too much noise.

Table S3. Affective ratings across picture categories and groups

	Controls		Patient 1		Patient 2	
	MS	SEM	S	Z	S	Z
Valence						
Negative	1.88	0.19	2.55	1.00	3.95	3.10
Neutral	5.50	0.17	5.30	-0.35	5.05	-0.79
Arousal						
Negative	6.81	0.58	5.15	-0.82	2.70	-2.04
Neutral	2.86	0.42	1.00	-1.27	1.00	-1.27

MS, mean score; SEM, standard error of the mean; S, individual score; Z, z-score.

Experiment 4

In the controls, social network size and social network complexity (41) scores were positively correlated (Spearman's $\rho = 0.68$; $p = 0.01$ two-tailed; Pearson's $r = 0.62$, $p = 0.01$ two-tailed, Figure S5). In order to integrate size and complexity of the social network in a single measure, composite scores were calculated in three steps: first, individual scores in each subscale were z-standardized within the control group $z_i = (x_i - \bar{x})/s$; in a second step, z-scores from both subscales were added for each individual: $z_{\text{sum}(i)} = z_{\text{complexity}(i)} + z_{\text{size}(i)}$; third, sum scores were z-standardized and transformed to a normal distribution with a mean of 100 and a standard deviation of 10, resulting in the final composite scores:

$$X_{\text{composite}(i)} = (z_{\text{sum}(i)} - \bar{z}_{\text{sum}(i)}) / s_{\text{sum}}$$

$$\text{where: } s_{\text{sum}}^2 = s_{\text{complexity}}^2 + s_{\text{size}}^2 + 2\text{Cov}_{(\text{complexity}, \text{sum})}$$

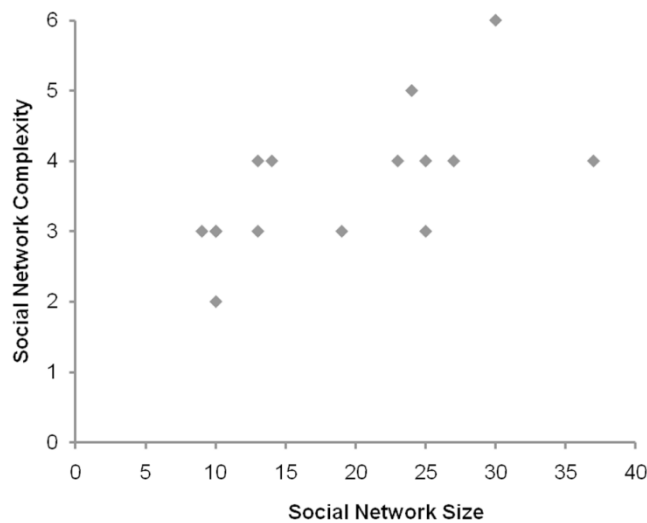


Figure S5. The cumulative count of Social Network Index questionnaire scores in controls. Empirical cumulative distribution function scores, as reported in the main article, were defined by $F_{\text{ecdf}}(x_i) = p(x \leq x_i)$. The empirical cumulative distribution function for a value x describes the proportion of values in a given set (e.g., study sample) that are less than or equal to x (in other words, it could be described as the 'area so far' function of the probability distribution). Thus, $F_{\text{ecdf}(x)} = 1$ indicates that x was the highest value in the entire sample, $F_{\text{ecdf}(x)} = 0$ corresponds to the lowest value, and $F_{\text{ecdf}(x)} = 0.5$ corresponds to the median.

Supplemental References

1. Hamada T, McLean WH, Ramsay M, Ashton GH, Nanda A, Jenkins T, *et al.* (2002): Lipoid proteinosis maps to 1q21 and is caused by mutations in the extracellular matrix protein 1 gene (ECM1). *Hum Mol Genet* 11:833–840.
2. Appenzeller S, Chaloult E, Velho P, de Souza EM, Araújo VZ, Cendes F, Li LM (2006): Amygdalae calcifications associated with disease duration in lipoid proteinosis. *J Neuroimaging* 16:154–156.
3. Hurlmann R, Patin A, Onur OA, Cohen MX, Baumgartner T, Metzler S, *et al.* (2010): Oxytocin enhances amygdala-dependent, socially reinforced learning and emotional empathy in humans. *J Neurosci* 30:4999–5007.
4. Strange BA, Hurlmann R, Dolan RJ (2003): An emotion-induced retrograde amnesia in humans is amygdala- and beta-adrenergic-dependent. *Proc Natl Acad Sci U S A* 100:13626–13631.
5. Hurlmann R, Wagner M, Hawellek B, Reich H, Pieperhoff P, Amunts K, *et al.* (2007): Amygdala control of emotion-induced forgetting and remembering. *Neuropsychologia* 45:877–884.
6. Hurlmann R, Schlaepfer TE, Matusch A, Reich H, Shah NJ, Zilles K, *et al.* (2009): Reduced 5-HT(2A) receptor signaling following selective bilateral amygdala damage. *Soc Cogn Affect Neurosci* 4:79–84.
7. Siebert M, Markowitsch HJ, Bartel P (2003): Amygdala, affect and cognition: evidence from 10 patients with Urbach-Wiethe disease. *Brain* 126:2627–2637.
8. Thornton HB, Nel D, van Honk J, Baker GA, Stein DJ (2008): The neuropsychiatry and neuropsychology of lipoid proteinosis. *J Neuropsychiatry Clin Neurosci.* 20:86–92.
9. Chan I, Liu L, Hamada T, Sethuraman G, McGrath JA (2007): The molecular basis of lipoid proteinosis: mutations in extracellular matrix protein 1. *Exp Dermatol* 16:881–890.
10. Hamada T, Wessagowit V, South AP, Ashton GH, Chan I, Oyama N, *et al.* (2003): Extracellular matrix protein 1 gene (ECM1) mutations in lipoid proteinosis and genotype-phenotype correlation. *J Invest Dermatol* 120:345–350.
11. Lupo I, Cefalu AB, Bongiorno MR, Daniele O, Valenti V, Noto D, *et al.* (2005): A novel mutation of the extracellular matrix protein 1 gene (ECM1) in a patient with lipoid proteinosis (Urbach-Wiethe disease) from Sicily. *Br J Dermatol* 153:1019–1022.
12. Wang CY, Zhang PZ, Zhang FR, Liu J, Tian HQ, Yu L (2006): New compound heterozygous mutations in a Chinese family with lipoid proteinosis. *Br J Dermatol* 155:470–472.
13. Chan I, Sethuraman G, Sharma VK, Bruning E, Hamada T, McGrath JA (2004): Molecular basis of lipoid proteinosis in two Indian sibs. *J Dermatol* 31:764–766.
14. Salih MA, Abu-Amero KK, Alrasheed S, Alorainy IA, Liu L, McGrath JA, *et al.* (2011): Molecular and neurological characterizations of three Saudi families with lipoid proteinosis. *BMC Med Genet* 12:31.
15. Horev L, Wollina DU, Potikha T, Hafner A, Ingber A, Liu L, *et al.* (2009): Lipoid proteinosis: identification of two novel mutations in the human ECM-1 gene and lack of genotype-phenotype correlation. *Acta Derm Venereol* 89:528–529.
16. Chan I, El-Zurghany A, Zendah B, Benghazil M, Oyama N, Hamada T, McGrath JA (2003): Molecular basis of lipoid proteinosis in a Libyan family. *Clin Exp Dermatol* 28:545–548.
17. Teive HA, Pereira ER, Zavala JA, Lange MC, de Paola L, Raskin S, *et al.* (2004): Generalized dystonia and striatal calcifications with lipoid proteinosis. *Neurology* 63:2168–2169.
18. Di Giandomenico S, Masi R, Cassandrini D, El-Hachem M, De Vito R, Bruno C, Santorelli FM (2006): Lipoid proteinosis: case report and review of the literature. *Acta Otorhinolaryngol Ital* 26:162–167.
19. Nasir M, Latif A, Ajmal M, Ismail M, Hameed A (2009): A novel homozygous 62-bp insertion in ECM1 causes lipoid proteinosis in a multigeneration Pakistani family. *Br J Dermatol* 161:688–690.
20. Hameed A, Nasir M, Ajmal M, Latif L (2009): Novel human pathological mutations. Gene symbol: ECM1. Disease: Lipoid Proteinosis. *Hum Genet* 126:336.
21. Stenson PD, Ball EV, Mort M, Phillips AD, Shiel JA, Thomas NS, *et al.* (2003): Human Gene Mutation Database (HGMD): 2003 update. *Hum Mutat* 21:577–581.

22. Mugler JPr, Brookeman JR (1991): Rapid three-dimensional T1-weighted MR imaging with the MP-RAGE sequence. *J Magn Reson Imaging* 1:561–567.
23. Hoult DI, Richards RE (1976): The signal-to-noise ratio of the nuclear magnetic resonance experiment. *J Magn Reson Imaging* 24:71–84.
24. Oros-Peusquens AM, Stoecker T, Amunts K, Zilles K, Shah NJ (2010): In vivo imaging of the human brain at 1.5 T with 0.6-mm isotropic resolution. *Magn Reson Imaging* 28:329–340.
25. von Stockhausen HM, Pietrzyk U, Herholz K (1998): "3D-Tool" - a software system for visualization and analysis of coregistered multimodality volume datasets of individual subjects. *Neuroimage* 7:S799.
26. Onur OA, Patin A, Mihov Y, Buecher B, Stoffel-Wagner B, Schlaepfer TE, *et al.* (2011): Overnight deprivation from smoking disrupts amygdala responses to fear. *Hum Brain Mapp* (in press) [doi: 10.1002/hbm.21293]
27. Lundqvist D, Flykt A, Ohman A (1998): Karolinska Directed Emotional Faces (KDEF) [Database of standardized facial images]. Department of Neurosciences, Karolinska Hospital, Stockholm.
28. Oosterhof N, Todorov A (2008): The functional basis of face evaluation. *Proc Natl Acad Sci U S A* 105:11087–11092.
29. Ashburner J, Friston KJ (2003): In: *Human Brain Function*. Frackowiak *et al.* (eds). Academic Press, London.
30. Evans AC, Marrett S, Neelin P, Collins L, Worsley K, Dai W, *et al.* (1992): Anatomical mapping of functional activation in stereotactic coordinate space. *Neuroimage* 1:43–53.
31. Holmes CJ, Hoge R, Collins L, Woods R, Toga AW, Evans AC (1998): Enhancement of MR images using registration for signal averaging. *J Comput Assist Tomogr* 22:324–333.
32. Friston KJ, Holmes AP, Worsley KJ, Poline JP, Frith CD, Frackowiak RSJ (1994): Statistical parametric maps in functional imaging: a general linear approach. *Hum Brain Mapp* 2:189–210.
33. Maldjian JA, Laurienti PJ, Burdette JB, Kraft RA (2003): An automated method for neuroanatomic and cytoarchitectonic atlas-based interrogation of fMRI data sets. *Neuroimage* 19: 1233–1239.
34. Maldjian JA, Laurienti PJ, Burdette JH (2004): Precentral gyrus discrepancy in electronic versions of the talairach atlas. *Neuroimage* 21:450–455.
35. Tzourio-Mazoyer N, Landeau B, Papathanassiou D, Crivello F, Etard O, Delcroix N, *et al.* (2002): Automated anatomical labeling of activations in SPM using a macroscopic anatomical parcellation of the MNI MRI single-subject brain. *Neuroimage* 15:273–289.
36. Henson R (2006): Comparing a single patient versus a group of controls. Available online at: http://www.mrc-cbu.cam.ac.uk/people/rik.henson/personal/Henson_Singlecase_06.pdf.
37. Fusar-Poli P, Placentino A, Carletti F, Landi P, Allen P, Surguladze S, *et al.* (2009): Functional atlas of emotional faces processing: a voxel-based meta-analysis of 105 functional magnetic resonance imaging studies. *J Psychiatry Neurosci* 34:418–432.
38. Lang PJ, Bradley MM, Cuthbert, BN (2008): International affective picture system (IAPS): Affective ratings of pictures and instruction manual. Technical Report A-8. University of Florida, Gainesville, FL.
39. Adolphs R, Tranel D, Damasio H, Damasio A (1994): Impaired recognition of emotion in facial expressions following bilateral damage to the human amygdala. *Nature* 372:669–672.
40. Fridlund A, Cacioppo J (1986): Guidelines for human electromyographic research. *Psychophysiology* 23:567–589.
41. Cohen S, Doyle WJ, Skoner DP, Rabin BS, Gwaltney JM (1997): Social ties and susceptibility to the common cold. *JAMA* 277:1940–1944.